PAPER

Check for updates

Short-range structure, the role of bismuth and property–structure correlations in bismuth borate glasses†

C. P. E. Varsamis,*[a] N. Makris,[b] C. Valvi[c] and E. I. Kamitsos [ID]*[b]

Bismuth-containing borate glasses, $x\mathrm{Bi_2O_3}$–$(1 - x)\mathrm{B_2O_3}$, were synthesized in the broad composition range $0.20 \leq x \leq 0.80$ by melting in Pt crucibles and splat-quenching between two metal blocks. Infrared reflectance spectra, measured in the range 30–5000 cm^{-1}, were transformed into absorption coefficient spectra and then deconvoluted into component bands to probe the glass structure as a function of composition. Integrated intensities of bands above 800 cm^{-1} were used in combination with mass and charge balance equations to quantify the short-range borate structure in terms of the molar fractions X_{4m}, X_{4o}, X_3, X_2, X_1 and X_0 for borate units $\mathrm{B\varnothing_4^-}$, $\mathrm{B\varnothing_2O_2^{3-}}$, $\mathrm{B\varnothing_3}$, $\mathrm{B\varnothing_2O^-}$, $\mathrm{B\varnothing O_2^{2-}}$ and $\mathrm{BO_3^{3-}}$, where $\varnothing$ and $\mathrm{O^-}$ denote bridging and non-bridging oxygen atoms. Borate tetrahedral units were found to be present in both the *meta*-borate, $\mathrm{B\varnothing_4^-}$, and *ortho*-borate, $\mathrm{B\varnothing_2O_2^{3-}}$, forms with $\mathrm{B\varnothing_4^-}$ constituting the dominating tetrahedral species for $0.20 \leq x \leq 0.70$. The $\mathrm{B\varnothing_2O_2^{3-}}$ units prevail at higher $\mathrm{Bi_2O_3}$ levels ($x > 0.7$), and coexist with their isomeric triangular borate species $\mathrm{BO_3^{3-}}$ ($\mathrm{B\varnothing_2O_2^{3-}} \rightleftharpoons \mathrm{BO_3^{3-}}$). The present IR results for the total molar fraction of borate tetrahedral units, $X_4 = X_{4m} + X_{4o}$, are in very good agreement with reported NMR results for the fraction of boron atoms in four-fold coordination, N_4. Besides evaluating X_{4m} and X_{4o}, the present work reports also for the first time the fractions of all types of triangular borate species X_{3-n} with $n = 0$, 1, 2 and 3. The IR region below 550 cm^{-1} was found to be dominated by the Bi–O vibrational activity in coexisting ionic (160–230 cm^{-1}) and distorted $\mathrm{BiO_6}$ sites (330–365 cm^{-1} and 475–510 cm^{-1}), a result reflecting the dual role of $\mathrm{Bi_2O_3}$ as glass-modifier and glass-former oxide. The latter role dominates in glasses exceeding 60 mol% $\mathrm{Bi_2O_3}$, and is consistent with the extended glass formation in the bismuth-borate system. The structural results were used to calculate the average number of bridging B–$\varnothing$ bonds per boron center, the average Bi–O and B–O single bond energy, and the atomic packing density of the studied glasses. These properties vary approximately linearly with $\mathrm{Bi_2O_3}$ content in the three regimes $0.2 \leq x \leq 0.4$, $0.4 < x \leq 0.6$ and $0.6 < x \leq 0.83$, and contribute collectively to the composition dependence of glass transition temperature.

[a] *Applied Physics Laboratory, Faculty of Engineering, University of West Attica, 250 Thivon, 112 41 Egaleo, Attica, Greece. E-mail: cvars@uniwa.gr*

[b] *Theoretical and Physical Chemistry Institute, National Hellenic Research Foundation, 48 Vass. Constantinou Ave., 116 35 Athens, Greece. E-mail: eikam@eie.gr*

[c] *Electronic Devices and Materials Laboratory, Department of Electrical and Electronics Engineering, University of West Attica, 250 Thivon, 112 41 Egaleo, Attica, Greece*

† Electronic supplementary information (ESI) available: Application of infrared spectroscopy for the calculation of the molar fractions of the borate species present in glass compositions $x = 0.50$ and 0.60 of the system $x\mathrm{Bi_2O_3}$–$(1 - x)\mathrm{B_2O_3}$. See DOI: 10.1039/d1cp00301a

1. Introduction

Bismuth borate glasses constitute a promising family of materials for contemporary technological applications. For more than two decades the majority of such applications involved the field of photonics,[1–15] while recent investigations recognize that the non-toxic bismuth borate glasses may replace radiation shielding concretes and lead-based commercial glasses for gamma ray and neutron radiation shielding applications.[16–18]

Early studies[19] suggested that potential alternatives to semiconductor materials with nonlinear optical properties could be transparent glasses with high linear refractive index. Thus, stable glassy systems having a broad forming range and containing highly polarizable metal ions are desirable; one possible candidate is the bismuth-borate system. The pioneering work on the complete phase diagram of the $\mathrm{Bi_2O_3}$–$\mathrm{B_2O_3}$ system by Levin and McDaniel[20] showed that stable glasses can be prepared with up to *ca.* 76 mol% $\mathrm{Bi_2O_3}$, whereas five crystalline compounds also exist with molar ratios of bismuth oxide to boron oxide of 1:4, 1:3, 3:5, 2:1 and 12:1. Among these

crystals, the monoclinic BiB_3O_6 shows exceptionally large linear and nonlinear optical coefficients.[21,22] More recent studies on glass formation and properties in the bismuth-borate system extended the glass forming range up to *ca.* 88.2 mol% Bi_2O_3 by employing the twin roller quenching technique.[23,24]

Glasses xBi_2O_3–$(1 - x)B_2O_3$ continue attracting interest mostly because of their unique linear and nonlinear optical properties which can be tuned by varying the Bi_2O_3 content over a broad composition range.[23–27] For example, the second order non-linear optical susceptibility induced by thermal poling was found to increase with increasing the Bi_2O_3 content,[8] and the third order optical non-linearity is one order of magnitude larger than that of silica glass and has a response time faster than 200 fs.[9] In addition, doping bismuth borate glasses with a variety of rare earth ions, like Dy^{3+}, Eu^{3+}, Tb^{3+} and Nd^{3+} makes them luminescence materials with potential applications in solid-state lasers and optical amplifiers.[11,12,15] Recently, bismuth-borate glasses have been used as suitable matrices for the incorporation of gold nanoparticles resulting in materials with high refractive index suitable for photonic applications.[14] Bismuth-borate glasses have also large and positive values of the thermo-optic coefficient (dn/dT), *i.e.* large changes of the refractive index with temperature, with dn/dT increasing with Bi_2O_3 content.[28]

The correlation of properties with composition and structure allows for the tuning of the glass response according to specific technological applications. Therefore, the investigation of chemical, physical/optical and structural properties of Bi_2O_3-containing borate glasses is of key importance and several efforts have been made in this direction.[29–38] In previous studies, a multitude of characterization techniques have been employed including XPS,[29,30] infrared,[29,32,33,38] Raman,[25,32–35] neutron diffraction,[31] and ^{11}B MAS NMR.[25,37]

It is widely documented that the structure of metal oxide-containing borate glasses consists of borate tetrahedral and triangular units; the number of non-bridging oxygen atoms on the latter units depends on the modification level of the borate network.[39–55] In the absence of metal oxides, *i.e.* pure B_2O_3 glass, the borate structure contains only neutral $BØ_3$ triangles (Ø denotes an oxygen atom bridging two boron centers), of which *ca.* 75% are arranged in planar six-membered boroxol rings.[56] Upon addition of metal oxide to B_2O_3, $BØ_3$ triangles are converted initially to charged tetrahedral units $BØ_4^-$. The further increase of metal oxide content results in the progressive depolymerization of the borate backbone, through the breaking of B–O–B linkages and the creation of non-bridging oxygen atoms (NBO, or O^-). The latter are formed mainly on charged triangular borate units which change gradually from $BØ_2O^-$ to $BØO_2^{2-}$ and to BO_3^{3-} *i.e.* from metaborate to pyroborate and to *ortho*-borate triangular moieties, respectively.[39–55]

Previous investigations on xBi_2O_3–$(1 - x)B_2O_3$ glasses revealed the coexistence of borate tetrahedral and triangular units for modification levels up to *ca.* $x = 0.70$.[25,31,34,37] For the quantification of the borate structure, the molar fraction of tetrahedral borate units, N_4, was obtained by NMR[25,37] and

neutron diffraction[31] techniques. The NMR results showed that N_4 exhibits a maximum value at about $x = 0.42$, while neutron diffraction data indicated a gradual increase of N_4 from $N_4 = 0.38$ at $x = 0.30$ to $N_4 = 0.48$ at $x = 0.67$. However, neither the nature of the borate triangles was unambiguously identified nor their molar fractions were obtained in previous studies;[25–31,34,36–38] due mostly to two reasons. First, the employed NMR and neutron diffraction techniques could not easily distinguish the different types of triangular borate units. Second, when infrared spectroscopy was used, by which the vibrational modes of different triangular borate units can be resolved,[44–50] the infrared spectra of bismuth-borate glasses were measured using the KBr pellet technique.[29,32–38] While this method allows for the derivation of qualitative information, it leads usually to partial hydrolysis of the dispersed glass, to ion-exchange phenomena and to the mixing of transmission and reflection responses; these factors lead to spectral distortions and to non-reproducible intensities of the infrared absorption bands.[45,57]

The literature overview presented above shows that a detailed mapping of the borate network structure as a function of bismuth oxide content is still lacking. We present here for the first time, to the best of our knowledge, a systematic investigation in the bismuth-borate glass system by means of infrared reflectance spectroscopy. This technique has been successfully applied in the past to study different families of glasses, to quantify their network structure and to reveal the nature and distribution of sites hosting the metal ions.[44–50,57] Specifically, the analysis of the mid-infrared spectra, *i.e.* above *ca.* 650 cm^{-1}, can facilitate the quantitative mapping of the borate structural units; whereas information about the oxide sites hosting the Bi ions can be deduced from the analysis of far-infrared profiles. This will permit to identify the role of Bi_2O_3 in borate glasses either as modifier and/or as glass-former oxide. The quantification of structure allows discussing the evolution of glass transition temperature on the basis of glass rigidity, as viewed in terms of the average number of bridging boron–oxygen bonds per boron center, the average boron–oxygen and bismuth–oxygen single bond energy and the atomic packing density of the bismuth-borate glasses.

2. Experimental

2.1. Glass preparation

Bismuth-borate glasses with the nominal composition xBi_2O_3–$(1 - x)B_2O_3$ were prepared by mixing appropriate stoichiometric amounts of high purity ($>99.5\%$) reagent-grade anhydrous Bi_2O_3 and B_2O_3 powders. Batches corresponding to approximately 5 g were thoroughly mixed, placed in Pt crucibles and melted for 15 minutes at temperatures between 800 and 1000 °C depending on composition. The use of Pt crucibles and low melting temperatures are crucial factors, because a previous investigation on glasses containing bismuth oxide showed that silica and porcelain crucibles are very strongly corroded when used for melting and this leads to alterations of glass

This journal is © the Owner Societies 2021

Phys. Chem. Chem. Phys., 2021, **23**, 10006–10020 | **10007**

composition.[58] The melts of this study were homogenized by frequent stirring, and glass samples were prepared by the conventional splat-quenching technique by quenching the melt between two polished stainless-steel blocks. With this preparation method, nine bismuth-borate compositions were obtained in bulk glass forms in the range $0.2 \leq x \leq 0.8$ ($x = 0.2, 0.3, 0.4, 0.5, 0.6, 0.65, 0.7, 0.75$ and 0.80). The glass specimens had thickness of about 1 mm with smooth and flat surfaces, suitable for specular reflectance measurements without any further treatment. The prepared glasses were light yellow to brownish with increasing the Bi_2O_3 content.

2.2. Infrared spectroscopy

Infrared (IR) reflectance spectra were measured on a vacuum Fourier-transform spectrometer (Bruker IFS 113v) at room temperature. A quasi-normal incidence mode ($11°$) was employed with an aluminum mirror as reference. Different infrared sources (globar and Hg arc lamp) and detectors (DTGS with KBr and polyethylene windows) were used to cover effectively the $30–5000$ cm^{-1} frequency range. Mid-infrared spectra ($400–5000$ cm^{-1}) were measured with a KBr beam splitter, whereas far-infrared spectra at frequencies below 700 cm^{-1} were collected using five different mylar beam splitters with thickness $3.5–50$ μm. Each spectrum, measured using a particular optic configuration, is the average of 200 scans with 2 cm^{-1} resolution. The final reflectance spectrum of each glass composition results from the appropriate merging of the six individual measured spectra to give a continuous spectrum in the $30–5000$ cm^{-1} range.

The measured reflectance spectra were analyzed by the Kramers–Kronig (KK) method to calculate the real, $n(\tilde{\nu})$, and imaginary, $k(\tilde{\nu})$, parts of the complex refractive index $\tilde{n}(\tilde{\nu}) = n(\tilde{\nu}) + ik(\tilde{\nu})$, where $\tilde{\nu}$ is the frequency in wavenumbers (cm^{-1}). The KK procedure requires extrapolation of the measured reflectance spectrum at the two limits $\tilde{\nu} \rightarrow 0$ and $\tilde{\nu} \rightarrow \infty$, as has been described in previous studies.[45,57] The results of this study are presented and discussed here in terms of the absorption coefficient spectra $\alpha(\tilde{\nu})$ calculated by $a(\tilde{\nu}) = 4\pi\tilde{\nu}k(\tilde{\nu})$. Then, the absorption coefficient spectra were deconvoluted into Gaussian component bands, $G_i(\tilde{\nu})$, according to the relationship:

$$\alpha(\tilde{\nu}) = \sum_{i=1}^{n} G_i(\tilde{\nu}) = \sum_{i=1}^{n} \frac{A_i}{w_i \sqrt{\pi/2}} \exp\left[-\frac{2(\tilde{\nu} - \nu_i)^2}{w_i^2}\right] \quad (1)$$

where the parameters ν_i, w_i, A_i denote the resonance frequency, width and integrated band intensity of each Gaussian component, respectively.[59] The deconvolution procedure relates to the determination of the best values of the adjustable parameters ν_i, w_i, A_i in order to obtain the most accurate description of the calculated $\alpha(\tilde{\nu})$ spectrum. The fitting procedure requires using, as a first step, the simplex algorithm followed by the application of the Levenberg–Marquardt algorithm, with a tolerance of 10^{-8}.[60] In the fitting procedure, the minimum number of component bands is used and, at the same time, the width values of the component bands that are assigned to the same vibrational mode

of a particular structural unit are restricted to differ by less than 10% for different glass compositions. By imposing this constraint, it becomes meaningful to extract a quantitative description for the glass speciation.

3. Results

The reflectance spectra of glasses $x\mathrm{Bi_2O_3}–(1 − x)\mathrm{B_2O_3}$ are depicted in Fig. 1 and 2 for $0.2 \leq x \leq 0.5$ and $0.6 \leq x \leq 0.8$ respectively. As the Bi_2O_3 content increases the far-IR activity shifts to higher frequencies and enhances relative to that in the mid-IR range. The far-infrared profiles of the studied glasses should result mainly from vibrational modes of Bi-containing oxide sites, while the mid-infrared activity arises from B–O vibrations in borate entities.[44–52]

A detailed consideration of the spectral profiles and their composition dependence will be presented next in the absorption coefficient formalism, $a(\tilde{\nu})$. The calculated $\alpha(\tilde{\nu})$ spectra are depicted in Fig. 3 and 4 after being normalized to their band maxima and appropriately shifted for better visualization.

3.1. Mid-infrared spectra

Inspection of Fig. 3 and 4 shows that all mid-infrared spectra exhibit three distinct absorption profiles, situated between ca. $600–750$ cm^{-1}, $750–1150$ cm^{-1} and $1150–1600$ cm^{-1}, with shape and relative intensity depending strongly on glass composition. According to previous studies,[44–52,57] the high-frequency IR envelope at ca. $1150–1600$ cm^{-1} originates from asymmetric B–O stretching vibration modes of borate triangular units, while the corresponding modes of tetrahedral borate units are active at lower frequencies ($750–1150$ cm^{-1}). Deformation modes of the borate units give rise to weaker absorption bands in the ca. $600–750$ cm^{-1} range. For example, the relatively narrow peaks at 700 and 710 cm^{-1} in Fig. 3 and 4 can be attributed to the out-of-plane bend of borate triangular units.
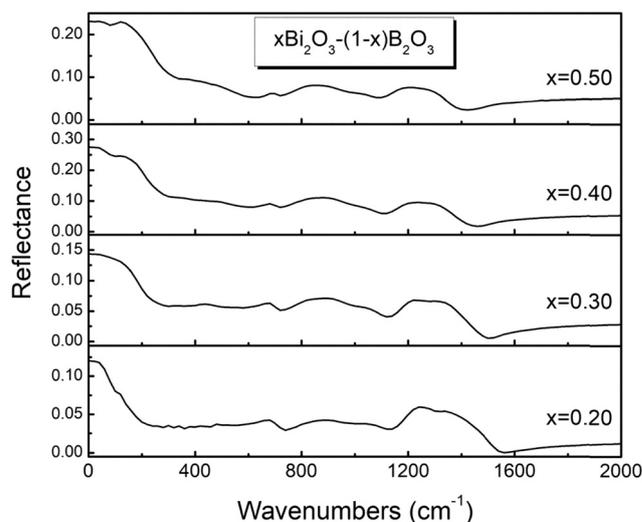

Fig. 1 Infrared reflectance spectra of glasses $x\mathrm{Bi_2O_3}–(1 − x)\mathrm{B_2O_3}$ with $x = 0.2, 0.3, 0.4$ and 0.5.

10008 | *Phys. Chem. Chem. Phys.*, 2021, **23**, 10006–10020

This journal is © the Owner Societies 2021
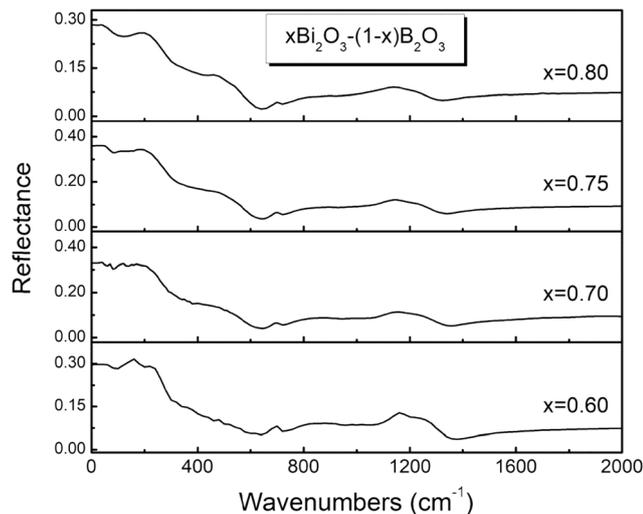
Fig. 2 Infrared reflectance spectra of glasses xBi$_2$O$_3$–$(1-x)$B$_2$O$_3$ with x = 0.6, 0.7, 0.75 and 0.8.
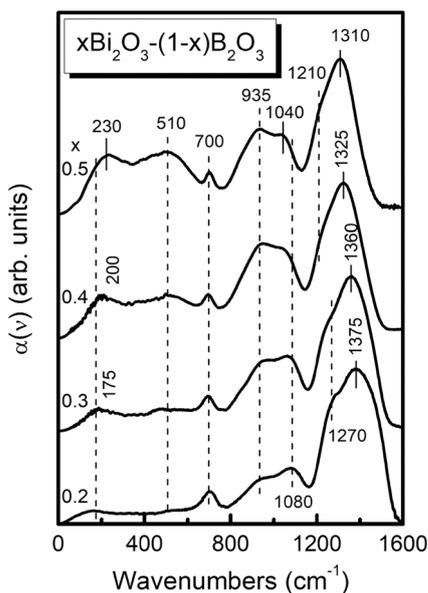
Fig. 3 Calculated absorption coefficient spectra, a($\bar{\nu}$), of glasses xBi$_2$O$_3$–$(1-x)$B$_2$O$_3$ for x = 0.2, 0.3, 04 and 0.5. All spectra are normalized to their maximum intensity value and shifted for better visualization.

It is observed that the high-frequency profile exhibits a red shift upon increasing the Bi$_2$O$_3$ content, the peak maxima shifting from 1375 to 1310 cm^{-1} for $0.2 \leq x \leq 0.5$ and from 1285 to 1240 cm^{-1} for $0.6 \leq x \leq 0.8$. In addition, the bandwidth of the high-frequency profile decreases progressively upon increasing the modification level. It is noted that pronounced red shifts of the high-frequency IR absorption envelopes were observed also in recent studies of Sr,Eu borate glasses[51] and highly modified Sr,Mn borate glasses.[61] These trends have been attributed to the progressive depolymerization of the borate network as *meta*-borate triangles, BØ$_2$O$^-$, in super-structural units transform progressively to pyroborate dimers,
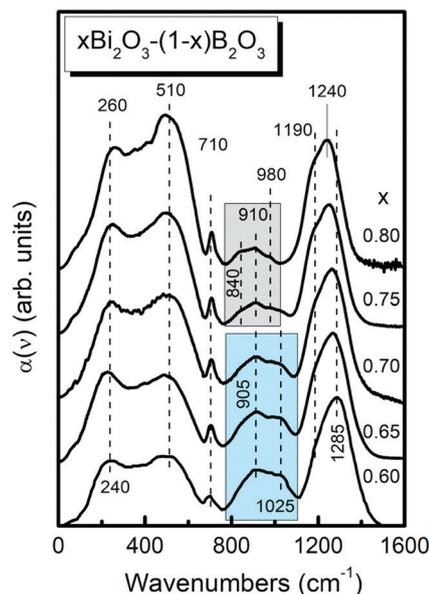

Fig. 4 Calculated absorption coefficient spectra, a($\bar{\nu}$), of glasses xBi$_2$O$_3$–$(1-x)$B$_2$O$_3$ for x = 0.6, 0.7, 0.75 and 0.8. All spectra are normalized to their maximum intensity value and shifted for better visualization.

B$_2$O$_5$$^{4-}$, and to *ortho*-borate monomers, BO$_3$$^{3-}$, upon increasing the degree of modification.

For x = 0.20 and 0.30, the high-frequency envelope is characterized by the presence of a peak at 1375–1360 cm^{-1} and a shoulder at *ca.* 1270 cm^{-1}, which signal the presence of *meta*-borate triangles, BØ$_2$O$^-$. In particular, the peak at 1375–1360 cm^{-1} can be attributed to the stretching of B–O$^-$ bonds and the lower-frequency shoulder to the stretching of B–Ø bonds in BØ$_2$O$^-$ triangles. Previous studies of lithium borate[45] and silver borate[47] glasses showed that replacement of a bridging oxygen (Ø) by a non-bridging one (O$^-$) in a BØ$_3$ triangle of D_{3h} symmetry to form a BØ$_2$O$^-$ unit will reduce the symmetry to C_{2v}, and this will split the doubly generate E' asymmetric stretching mode under D_{3h} into two IR-active components of A$_1$ and B$_2$ symmetry. This phenomenon is manifested in the infrared absorption spectra of Li- and Ag-borate glasses by the appearance of two component bands in the 1220–1250 cm^{-1} and 1435–1450 cm^{-1} frequency ranges, attributed to the stretching of B–Ø and B–O$^-$ bonds of BØ$_2$O$^-$ units, respectively. Similar results were found in recent studies of highly modified borate glasses.[51,52,61] The observed decrease in frequency of the B–O$^-$ stretching in BØ$_2$O$^-$ units (1375–1360 cm^{-1}) in the present study suggests stronger inter-actions between Bi^{3+} ions and non-bridging oxygens, which consequently weakens the strength in B–O$^-$ bonding and increases the degree of covalence in Bi–O bonding.

For compositions with x = 0.4 and 0.5, the progressive downshift of the peak frequency to 1325 and 1310 cm^{-1} is attributed to the formation of pyroborate dimers, B$_2$O$_5$$^{4-}$, in accordance with previous findings in highly modified borate glasses.[45,51,52,61] As shown in Fig. 3, this downshift is accompanied by the presence of a shoulder at *ca.* 1210 cm^{-1}. Such features are typical for the asymmetric stretching of the

This journal is © the Owner Societies 2021

Phys. Chem. Chem. Phys., 2021, **23**, 10006–10020 | **10009**

terminal B–O$^-$ bonds (1325–1310 cm^{-1}) and the B–O–B bridges (1210 cm^{-1}) in pyroborate units.[45,51,52,61]

At large Bi$_2$O$_3$ contents ($0.6 \leq x \leq 0.8$, Fig. 4) the high frequency envelope consists of two distinct features, a peak at 1285–1240 cm^{-1} and a shoulder at *ca.* 1190 cm^{-1}. These spectral characteristics signal the formation of *ortho*-borate units, BO$_3^{3-}$,[45,51,61] as they can be assigned to the splitting of the doubly degenerate ν_3 asymmetric stretching mode of such units. The presence of BO$_3^{3-}$ units is also manifested by the well-defined peak around 710 cm^{-1} that is due to the their out-of-plane bending mode.[45,51,61]

The absorption envelope of BØ$_4^-$ tetrahedral units, between *ca.* 750 to 1150 cm^{-1}, appears to gain its maximum intensity relative to the high-frequency envelope for the composition $x = 0.4$ (Fig. 3), indicating a maximum fraction of BØ$_4^-$ units. At higher Bi$_2$O$_3$ contents, the 750–1150 cm^{-1} envelop loses gradually intensity indicating the destruction of BØ$_4^-$ units in favor of other structural entities. For $x = 0.75$ and 0.80, this mid-frequency absorption profile is substantially narrowed by almost 100 cm^{-1} and is characterized by the appearance of peaks at around 840, 910 and 980 cm^{-1}. Previous studies of *ortho*-borate crystals YBO$_3$,[62] GdBO$_3$,[63] EuBO$_3$, TbBO$_3$ and DyBO$_3$[64] having the vaterite type structure, that consists of BØ$_2$O$_2^{3-}$ tetrahedra arranged in B$_3$O$_9^{9-}$ rings, showed that the strongest infrared activity is in the 800–1150 cm^{-1} range with sharp peaks at *ca.* 870, 920 and 1010 cm^{-1}. Along the same lines, previous studies of superionic AgI-containing *ortho*-borate glasses,[65] Sr,Eu *ortho*-borate glasses[51] and highly modified Sr,Mn borate glasses[52] supported the existence of BØ$_2$O$_2^{3-}$ tetrahedral units at very high modification levels. For convenience, the assignments of the infrared bands discussed here are summarized in Table 1 as a function of Bi$_2$O$_3$ content.

A key finding of this study is that the structure of bismuth-borate glasses with modification level higher than $x = 0.70$ contains *ortho*-borate tetrahedra BØ$_2$O$_2^{3-}$ in coexistence with *ortho*-borate triangles BO$_3^{3-}$. These species are present in equilibrium because they are chemically isomeric, *i.e.* BØ$_2$O$_2^{3-} \rightleftharpoons$

BO$_3^{3-}$. It is noted also that the formation of BØ$_2$O$_2^{3-}$ tetrahedral species, which have two bridging (Ø) and two non-bridging (O$^-$) oxygen atoms, is compatible with the very broad glass-forming region $0.2 \leq x \leq 0.8$ in xBi$_2$O$_3$–$(1 - x)$B$_2$O$_3$ glasses. While the nominal *ortho*-borate composition (O/B = 3/1) corresponds to $x = 0.5$ in such glasses, the glass-forming region extends well-above this limit and reaches $x = 0.80$ by splat-quenching and even $x = 0.88$ by twin roller quenching.[23] This is in contrast to lithium-borate glasses xLi$_2$O–$(1 - x)$B$_2$O$_3$ for which glass formation by splat-quenching was possible up to $x = 0.73$, *i.e.* the pure *ortho*-borate glass composition ($x = 0.75$) was not achieved due to partial crystallization at $x = 0.73$.[45] This can be rationalized in terms of the main structural difference between these two glass systems; while BO$_3^{3-}$ triangles are the only borate species present in Li-*ortho*-borate, they coexists with their isomeric tetrahedral *ortho*-borate units BØ$_2$O$_2^{3-}$ in highly-modified Bi-borate glasses and this appears to prevent crystallization.

The above findings are in line with reported structures and infrared spectra of crystalline bismuth-borate compounds of similar stoichiometry. Starting with the low Bi$_2$O$_3$ content $x = 0.20$, the structure of the Bi$_2$B$_8$O$_{15}$ crystal consists of infinite chains of *meta*-borate rings B$_3$O$_6^{3-}$ linked together by BiO$_6$ octahedra, BØ$_3$ triangles and BØ$_4^-$ tetrahedra.[66] The corresponding mid-IR transmittance spectrum[35] exhibits the two characteristic bands of BØ$_2$O$^-$ units centered at *ca.* 1250 and 1360 cm^{-1}, and several peaks in the 800–1100 cm^{-1} range due to BØ$_4^-$ tetrahedra. The BiB$_3$O$_6$ crystal, corresponding to $x = 0.25$ and having the *meta*-borate stoichiometry (O/B = 2/1), consists of infinite chains of alternating *meta*-borate triangles BØ$_2$O$^-$ and *meta*-borate tetrahedra BØ$_4^-$ in a 1:1 ratio.[67] The mid-IR spectrum of BiB$_3$O$_6$ crystal[35] resembles that of Bi$_2$B$_8$O$_{15}$, with characteristic absorptions of *meta*-borate triangular and tetrahedral species.

The Bi$_3$B$_5$O$_{12}$ crystal structure, $x = 0.375$, contains Bi^{3+} cations, isolated pentaborate type anions B$_5$O$_{11}^{7-}$ and O^{2-} anions not bonded to any boron–oxygen group and situated in the centers of isolated OBi$_3$ triangles.[68] The isolated

Table 1 Assignments of infrared bands of glasses xBi$_2$O$_3$–$(1 - x)$B$_2$O$_3$. Frequency values of the component bands resulted from the deconvolution of the IR spectra are given in Table 2

Composition	Frequency range (cm^{-1})	Assignment
$x = 0.2$–0.8	150–230	Bi–O stretch in ionic bismuth–oxygen sites
	325–380	Asymmetric bend in distorted BiO$_6$ sites
	480–510	Asymmetric stretch in distorted BiO$_6$ sites
	595–615	In-plane bend of triangular borate units
	695–710	Out-of-plane bend of triangular borate units
$x = 0.20$–0.75	820–850	B–Ø stretch in BØ$_4^-$ units
	910–960	
	1020–1100	
$x = 0.60$–0.80	810–820	B–Ø ring and B–O$^-$ terminal stretch in [B$_3$O$_9$]$^{9-}$ rings
	900–910	of BØ$_2$O$_2^{3-}$ tetrahedral units
	1025–1030	
$x = 0.30$–0.65	1170–1215	B–O–B stretch in pyroborate units, BØO$_2^{2-}$
$x = 0.20$–0.40	1215–1260	B–Ø stretch in BØ$_2$O$^-$ units
$x = 0.70$–0.80	1155–1200	B–O$^-$ stretch in *ortho*-borate units, BO$_3^{3-}$
	1240–1290	
$x = 0.30$–0.65	1270–1330	B–O$^-$ stretch in pyroborate units, BØO$_2^{2-}$
$x = 0.20$–0.40	1330–1390	B–O$^-$ stretch in BØ$_2$O$^-$ units
$x = 0.20$	1480	B–Ø stretch in BØ$_3$ units

10010 | *Phys. Chem. Chem. Phys.*, 2021, **23**, 10006–10020

This journal is © the Owner Societies 2021

pentaborate type anions are formed by two condensed rings sharing a $BØ_4^-$ tetrahedron; one ring consists of this $BØ_4^-$ tetrahedron and two $BØ_2O^-$ triangles and the other involves the common $BØ_4^-$ tetrahedron bonded to a $BØ_2O^-$ triangle and to a $BØ_2O_2^{3-}$ tetrahedron.[68] The mid-IR transmittance spectrum of the $Bi_3B_5O_{12}$ crystal[35] exhibits a broad band centered at *ca.* 1320 cm^{-1} characteristic of $BØ_2O^-$ triangles, bands in the range 1030–1125 cm^{-1} for $BØ_4^-$ tetrahedral units and well defined bands at 840 and 938 cm^{-1} consistent with the existence of $BØ_2O_2^{3-}$ tetrahedra.

The structures of the crystalline compounds $BiBO_3$ (*ortho*-borate, $x = 0.50$) and $Bi_4B_2O_9$ ($x = 0.67$) contain discrete planar *ortho*-borate triangles, BO_3^{3-}.[69,70] The mid-IR transmittance spectra[35] of these two crystals can be fully described in terms of bands attributed to BO_3^{3-} vibrational modes; these include the B–O asymmetric stretch (broad envelope in the 1100–1300 cm^{-1} range), and out-of-plane bend at 690 cm^{-1}. The presence of multiple bands in the 1100–1300 cm^{-1} envelope arises from the low positional symmetry and the existence of non-equivalent sites for the *ortho*-borate triangles in the crystal structure, which remove the degeneracy of the asymmetric stretching vibration mode of the BO_3^{3-} units.

To summarize this section, our mid-IR structural analysis for four-fold coordinated B atoms in Bi-borate glasses suggests the presence of *meta*-borate tetrahedral units, $BØ_4^-$, for glasses with $0.2 \leq x \leq 0.70$, with *ortho*-borate tetrahedral units, $BØ_2O_2^{3-}$, prevailing at higher modification levels. Units with three-fold coordinated B atoms include the *meta*-borate triangles, $BØ_2O^-$, dominating in glasses with $x = 0.2$ and 0.3, and pyroborate dimers, $B_2O_5^{4-}$, for $x = 0.3$ to $x = 0.6$, while the *ortho*-borate monomers, BO_3^{3-}, constitute the majority of triangular borate species for $x \geq 0.50$.

3.2. Far-infrared spectra

Information on the bonding of metal cation in glass can be deduced from the far-IR spectral region, where vibrations of metal ions against their sites in the glass network are active.[44,45,52,57,61,65] As seen in Fig. 3 and 4, introduction of Bi_2O_3 in the borate glass causes the progressive evolution of a complex absorption profile which extends up to *ca.* 670 cm^{-1}. The contribution of this profile to the entire infrared response increases with Bi_2O_3 addition, suggesting that its origin should be traced mainly to vibration modes involving Bi cations.

Inspection of Fig. 3 shows that for the lower modification levels, $x = 0.2$–0.4, the far-IR profile appears to consist mainly of a low-frequency band with peak frequency increasing from about 160 cm^{-1} ($x = 0.20$) to 200 cm^{-1} ($x = 0.40$). For the $x = 0.50$ glass, the low-frequency band about 220 cm^{-1} is in co-existence with a higher-frequency component centered at about 510 cm^{-1}. These two features dominate the far-infrared region for the rest of glass compositions, $0.60 \leq x \leq 0.80$, as depicted in Fig. 4. In addition, the first peak at about 240 cm^{-1} appears to loss intensity at higher Bi_2O_3 contents in favor of the peak at about 510 cm^{-1}, which at $x = 0.80$ becomes the dominant feature of the entire IR spectrum.

We note that an infrared and Raman study of crystalline α-Bi_2O_3 and bismuth oxide derivatives with sillenite structure

showed strong infrared activity in the 400–600 cm^{-1} range, assigned to the stretching of Bi–O bonds in BiO_6 polyhedra.[71] Similarly, studies on multicomponent bismuthate glasses assigned the far-IR absorption centered around 480 cm^{-1} to the Bi–O stretching in strongly distorted BiO_6 octahedral moieties.[32,33,36,72,73] The existence of BiO_6 octahedra was proposed also in Raman studies of unconventional lithium-bismuthate glasses[74] and ternary Bi_2O_3-containing phosphate and borate glasses,[75] in a neutron and X-ray diffraction study of Bi_2O_3–Ga_2O_3 glasses,[76] and in a structural study of Bi_2O_3–Fe_2O_3 glasses by X-ray diffraction, IR, EPR and Mossbauer spectroscopies.[77] On these grounds, we associate the band at *ca.* 500 cm^{-1} with the formation of BiO_6 octahedral units in the bismuth-borate glasses of this study.

The lower-frequency peak in the 160–240 cm^{-1} range can be attributed to vibrations of Bi cations against their ionic sites formed by oxygen atoms of the glass network. This assignment is in line with a plethora of previous investigations on metal oxide-containing borate glasses by both experimental and molecular simulations techniques.[44–52,57,61,65,78–81]

4. Discussion

4.1. Quantification of the short-range borate structure

The previously described qualitative picture for the evolution of the borate structure with Bi_2O_3 content can be further elaborated to determine the borate speciation expressed as molar fractions of the various borate entities. To this aim, we proceed by considering the deconvolution of the absorption coefficient spectra $\alpha(\check{\nu})$ according to eqn (1). Representative deconvoluted $\alpha(\check{\nu})$ spectra are depicted in Fig. 5 for $x = 0.2$ and $x = 0.4$ and in Fig. 6 for the $x = 0.65$ and $x = 0.80$ compositions, whereas the fitting parameters of the component bands are listed in Table 2 for all glass compositions.

In the following, we focus on the bands 1–6 in the 750–1600 cm^{-1} range which originate from the stretching vibration modes of borate units and use the notation X_i for the molar fraction of the unit having i bridging oxygen atoms per boron. Thus, X_{4m} denotes the molar fraction of *meta*-borate tetrahedral unit, $BØ_4^-$, and X_3, X_2, X_1, X_0 the molar fractions of $BØ_3$, $BØ_2O^-$, $BØO_2^{2-}$ and BO_3^{3-} triangular units, respectively.

For glass compositions $0.20 \leq x \leq 0.40$, mass and charge balance considerations give:

$$\sum_i X_i = 1 \tag{2}$$

$$X_{4m} + X_2 + 2X_1 + 3X_0 = \frac{3x}{1-x} \tag{3}$$

Denoting by A_j the integrated intensity of the j-th component band normalized by the total integrated intensity in the 750–1600 cm^{-1} range, the quantities A_j and X_i are related as follows:

$$A_j = \sum_i X_i a_i \tag{4}$$

where a_i is the normalized absorption coefficient of the particular vibration mode of a borate unit involved in the j-th
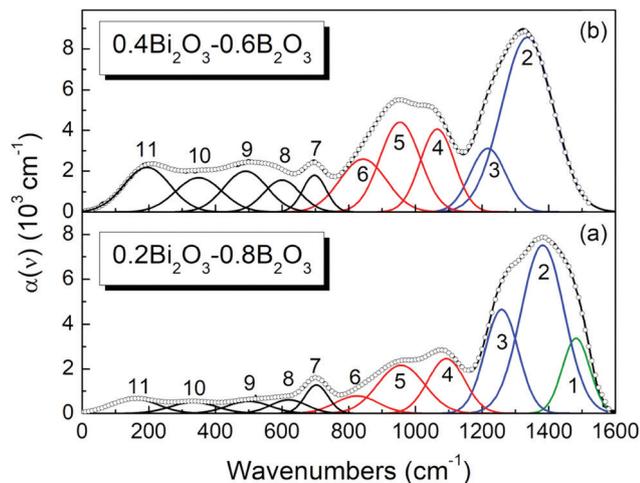
This journal is © the Owner Societies 2021

Phys. Chem. Chem. Phys., 2021, **23**, 10006–10020 | **10011**

Fig. 5 Deconvolution into Gaussian component bands of the infrared absorption coefficient spectra, a($\tilde{v}$), of glasses $x\mathrm{Bi_2O_3}-(1-x)\mathrm{B_2O_3}$ with x = 0.2 (a) and 0.4 (b). Black solid lines represent the experimental spectra and circle symbols (○) the simulated spectra. Gaussian component bands are colored as follows; ▬: band 1 attributed to $\mathrm{B\varnothing_3}$ triangles (x = 0.2), ▬: bands 2 and 3 attributed to $\mathrm{B\varnothing_2O^-}$ (x = 0.2) or to $\mathrm{B\varnothing O_2^{2-}}$ and $\mathrm{BO_3^{3-}}$ triangles (x = 0.4), ▬: bands 4–6 attributed to $\mathrm{B\varnothing_4^-}$ tetrahedral units. For assignments of bands 7–11 see text and Table 2.
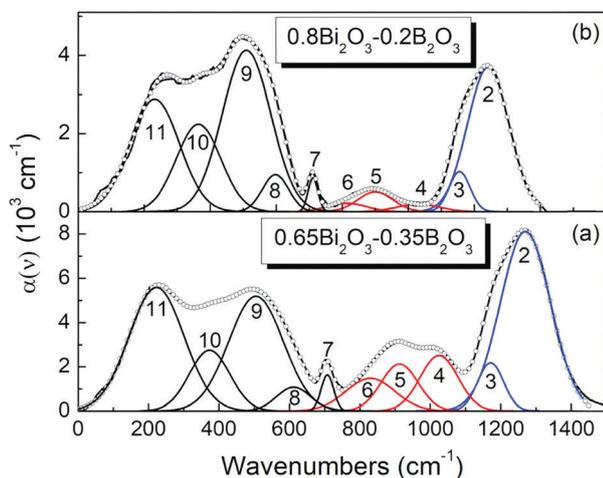

Fig. 6 Deconvolution into Gaussian component bands of the infrared absorption coefficient spectra, a($\tilde{v}$), of glasses $x\mathrm{Bi_2O_3}-(1-x)\mathrm{B_2O_3}$ with x = 0.65 and 0.80. Black solid lines represent the experimental spectra and circle symbols (○) the simulated spectra. Gaussian component bands are colored as follows; ▬: bands 2 and 3 attributed to $\mathrm{BO_3^{3-}}$ triangles, ▬: bands 4–6 attributed to $\mathrm{B\varnothing_4^-}$ tetrahedral units. For assignments of bands 7–11 see text and Table 2.

component band.[47] In eqn (4) the summation extends over the different borate units that contribute to the activity of the j-th component band.

Starting with the x = 0.20 glass composition, Fig. 5 shows that the 750–1600 cm^{-1} range is best fitted with six component bands. According to Section 3.1, the three bands at 1093, 957 and 824 cm^{-1} are due to $\mathrm{B\varnothing_4^-}$ tetrahedra, whereas the components at *ca.* 1382 and 1258 cm^{-1} are due to the

stretching of B–O$^-$ and B–Ø bonds in $\mathrm{B\varnothing_2O^-}$ units, respectively. The remaining band at 1482 cm^{-1} originates from the stretching of B–Ø bonds in neutral $\mathrm{B\varnothing_3}$ triangles. This assignment is consistent with the infrared spectrum of bure $\mathrm{B_2O_3}$ glass that exhibits a similar feature at *ca.* 1500 cm^{-1}.[45] Following these assignments, eqn (2) and (3) take the forms:

$$X_{4m} + X_3 + X_2 = 1 \tag{5}$$

$$X_{4m} + X_2 = \frac{3x}{1-x} = \frac{0.6}{0.8} = 0.75 \tag{6}$$

From the above equations, we obtain directly the molar fraction of $\mathrm{B\varnothing_3}$ triangles, X_3 = 0.25. Also, it is reasonable to assume that $a_{\mathrm{B-\varnothing}}$ values for B–Ø bond stretching in either $\mathrm{B\varnothing_2O^-}$ or $\mathrm{B\varnothing_3}$ units do not differ appreciably. In that case, eqn (4) for the component bands at 1258 and 1482 cm^{-1} leads to $A_{1258} = X_2 a_{\mathrm{B-\varnothing}}$ and $A_{1482} = X_3 a_{\mathrm{B-\varnothing}}$. Then, division of the latter equations by members and substitution of the integrated intensity values from Table 2 gives:

$$\frac{A_{1258}}{A_{1482}} = 1.68 = \frac{X_2}{X_3} \Rightarrow X_2 = 1.68 \cdot X_3 = 0.42 \tag{7}$$

Using the above result, the $a_{\mathrm{B-\varnothing}}$ value can be estimated: $a_{\mathrm{B-\varnothing}} = \frac{A_{1258}}{X_2} = 0.4624$ cm^{-2}. The obtained values for X_2 and X_3 and eqn (5) give the molar fraction of *meta*-borate tetrahedral units X_{4m} = 0.33.

The fitting results in Table 2 indicate that for x = 0.30 the 800–1600 cm^{-1} range is best fitted with five component bands (Fig. 5, bands 2–6). The first three bands at 1079, 957 and 820 cm^{-1} are due to $\mathrm{B\varnothing_4^-}$ tetrahedra, whereas the components at *ca.* 1393 and 1263 cm^{-1} are due to the stretching of B–O$^-$ and B–Ø bonds of $\mathrm{B\varnothing_2O^-}$ and $\mathrm{B\varnothing O_2^{2-}}$ units, respectively. For the x = 0.30 glass, eqn (2) and (3) give:

$$X_{4m} + X_2 + X_1 = 1 \tag{8}$$

$$X_{4m} + X_2 + 2X_1 = \frac{3x}{1-x} = \frac{0.9}{0.7} = 1.286 \tag{9}$$

Subtracting eqn (8) from eqn (9) gives immediately X_1 = 0.286. Moreover, eqn (4) for the component at 1263 cm^{-1} takes the form $A_{1263} = (X_2 + X_1)a_{\mathrm{B-\varnothing}}$ and by using the fitting values of Table 2 we obtain: $A_{1263} = (X_2 + X_1)a_{\mathrm{B-\varnothing}} \Rightarrow X_2 + X_1 = \frac{A_{1263}}{a_{\mathrm{B-\varnothing}}} = 0.592$. Thus, the calculated molar fractions of the borate units are X_1 = 0.286, X_2 = 0.306, X_{4m} = 0.408.

For the x = 0.40 composition, the 800–1600 cm^{-1} range is best fitted with five component bands. The first three at 1066, 952 and 842 cm^{-1} are typical for $\mathrm{B\varnothing_4^-}$ tetrahedra, while the two remaining components at 1331 and 1214 cm^{-1} originate from the vibrations of both $\mathrm{B\varnothing O_2^{2-}}$ and $\mathrm{BO_3^{3-}}$ units. Eqn (2) and (3) take now the following forms:

$$X_{4m} + X_1 + X_0 = 1 \tag{10}$$

$$X_{4m} + 2X_1 + 3X_0 = \frac{3x}{1-x} = \frac{1.2}{0.6} = 2 \tag{11}$$

These equations are easily reduced to:

10012 | *Phys. Chem. Chem. Phys.*, 2021, **23**, 10006–10020

This journal is © the Owner Societies 2021

Table 2 Deconvolution parameters of the $\alpha(\tilde{\nu})$ spectra of glasses $x\text{Bi}_2\text{O}_3-(1-x)\text{B}_2\text{O}_3$; resonance frequency ν_i (cm^{-1}), width w_i (cm^{-1}) and integrated intensity A_i (10^4 cm^{-2})

x	0.20	0.30	0.40	0.50	0.60	0.65	0.70	0.75	0.80
ν_1	1481.9								
w_1	82.1								
A_1	34.74								
ν_2	1382.0	1393.0	1331.0	1315.3	1290.8	1270.0	1265.2	1251.2	1242.1
w_2	130.0	136.3	159.6	143.9	137.1	142.1	135.4	134.6	126.2
A_2	122.57	115.4	176.0	109.5	168.1	144.5	99.0	93.0	58.5
ν_3	1258.8	1262.8	1213.9	1199.3	1185.0	1171.4	1166.6	1158.2	1155.5
w_3	100.0	140.6	93.1	101.7	87.4	73.7	68.3	65.0	63.5
A_3	58.4	85.5	30.0	27.4	33.6	20.2	13.8	12.9	8.2
ν_4	1093.1	1078.8	1066.0	1060.5	1030.0	1025.0	1021.1	1024.4	1030.0
w_4	110.0	90.2	107.1	88.5	109.9	107.9	109.5	105.2	130.0
A_4	34.0	32.7	55.3	23.1	48.8	34.1	18.9	10.7	3.2
ν_5	957.3	957.0	952.1	942.7	927.1	912.8	908.3	909.1	900.0
w_5	140.0	140.0	120.0	147.0	99.1	104.9	103.7	114.0	107.3
A_5	38.0	62.7	65.4	59.4	31.7	28.0	16.5	14.6	6.8
ν_6	824.1	820.0	841.8	820.5	850.0	830.0	820.0	810.0	813.9
w_6	130.0	110.0	140.0	130.0	126.0	140.0	150.0	139.7	119.1
A_6	12.8	16.0	44.7	16.6	40.0	26.0	15.0	8.3	3.3
ν_7	703.2	697.1	697.3	705.3	703.6	707.5	709.6	709.9	711.1
w_7	69.2	70.6	70.6	54.3	59.9	35.9	32.2	30.0	29.7
A_7	11.1	13.3	15.8	7.1	13.3	7.3	4.6	4.4	3.2
ν_8	609.9	598.1	600.2	607.9	597.3	615.6	599.7	600.0	597.8
w_8	110.0	108.6	110.0	120.0	90.0	92.1	100.8	84.3	79.2
A_8	9.9	13.2	21.6	19.0	20.6	12.1	15.2	11.1	9.4
ν_9	475.0	480.0	490.0	493.2	495.0	505.0	500.1	505.8	510.0
w_9	120.0	110.7	130.0	140.0	150	155.0	150.0	151.7	147.0
A_9	8.2	13.0	32.8	37.0	96.1	102.9	77.0	92.5	76.1
ν_{10}	330.0	341.4	350.0	356.1	357.3	365.0	368.4	360.7	365.0
w_{10}	120.8	140.0	137.5	140.0	125	120.0	130.0	130.0	135.0
A_{10}	7.1	13.0	28.6	27.5	44.9	43.9	37.6	46.0	37.9
ν_{11}	161.5	185.3	195.5	209.6	225.0	220.0	230.8	225.4	232.0
w_{11}	145.2	130.0	139.0	140.0	137.5	150.0	150.0	140.0	150.0
A_{11}	12.1	16.9	38.3	38.3	81.6	103.9	74.1	72.6	54.2

$$X_{4m} = X_0 \tag{12}$$

$$X_1 + 2X_0 = 1 \tag{13}$$

Eqn (11) shows that the glass $x = 0.40$ has the nominal pyroborate composition, with two negative charges per boron on the average. Therefore, the presence of the undermodified $\text{B}\varnothing_4^-$ tetrahedra (X_{4m}) must be counterbalanced by the existence of the overmodified *ortho*-borate BO_3^{3-} triangles (X_0). This is achieved through the following disproportionation reaction of pyroborate dimers:

$$\text{B}_2\text{O}_5^{4-} \rightarrow \text{B}\varnothing_4^- + \text{BO}_3^{3-} \tag{14}$$

The proposed reaction (14) is in agreement with the provision of eqn (12).

To proceed further, we note that for compositions with $x \geq 0.65$ the only borate triangles present are the BO_3^{3-} units. Also, we observe that for the two component bands attributed to BO_3^{3-} units, due to the splitting of their doubly degenerate ν_3 asymmetric stretching mode, the results of Table 2 indicate that the ratio of the integrated intensities of the low (1155–1170 cm^{-1}) vs. the high (1240–1270 cm^{-1}) frequency component band attributed to BO_3^{3-} units is constant and equal to 0.14 for $x \geq 0.65$. This was a constraint imposed in the fitting procedure in order to minimize the residual between experimental and simulated data in the $x = 0.65$ up to $x = 0.80$

composition range. With this constraint in mind, we return to composition $x = 0.40$ for which eqn (4) gives for the two components at 1331 and 1214 cm^{-1} the relations:

$$A_{1331} = (X_1 + X_0)a_{\text{B-O}^-} \tag{15a}$$

$$A_{1214} = X_1 a_{\text{B-}\varnothing} + 0.14X_0 a_{\text{B-O}^-} \tag{15b}$$

where $a_{\text{B-O}^-}$ is the normalized absorption coefficient for B–O$^-$ bond stretching in either $\text{B}\varnothing\text{O}_2^{2-}$ or BO_3^{3-} units. After substitution of $a_{\text{B-O}^-}$ from eqn (15a) and using $X_1 + 2X_0 = 1$ from eqn (13), the eqn (15b) then yields the following trinomial expression:

$$X_1^2 a_{\text{B-}\varnothing} + X_1(a_{\text{B-}\varnothing} - 0.14A_{1331} - A_{1214}) + 0.14A_{1331} - A_{1214} = 0 \tag{16}$$

The positive root of the above equation is $X_1 = 0.139$ and, as follows from eqn (12) and (13), $X_{4m} = X_0 = 0.43$. In addition, for the normalized absorption coefficient for B–O$^-$ bond stretching in either $\text{B}\varnothing\text{O}_2^{2-}$ or BO_3^{3-} units one obtains the value $a_{\text{B-O}^-} = 0.785$ cm^{-2}.

As mentioned in Section 3.1 and shown in Fig. 4, the borate speciation for glasses with $x = 0.50$ and 0.60 involves $\text{B}\varnothing\text{O}_2^{2-}$ and BO_3^{3-} trigonal units and borate tetrahedra in the form of either $\text{B}\varnothing_2\text{O}_2^{3-}$ or $\text{B}\varnothing_4^-$. The evaluation of molar fractions is based now on the mass balance equation, eqn (3), and on eqn (15), by adopting the previously calculated values for

$a_{\text{B−O−}} = 0.785 \text{ cm}^{-2}$ and $a_{\text{B−Ø}} = 0.4624 \text{ cm}^{-2}$ and the results of fitting for the normalized integrated intensities. In fact, a pair of equations similar to eqn (15) applied for the first two component bands, 1290–1315 cm^{-1} and 1185–1199 cm^{-1}, can be solved to obtain first the molar fractions X_1 and X_0 of $BØO_2^{2-}$ and BO_3^{3-} units. Then, the remaining molar fraction of borate tetrahedra results from the mass balance equation. With this procedure the calculated molar fractions for $x = 0.50$ are $X_1 = 0.145$, $X_0 = 0.447$ and $X_4 = 0.408$, whereas for $x = 0.60$ the corresponding values are $X_1 = 0.089$, $X_0 = 0.576$ and $X_4 = 0.335$. Details for the calculation of molar fraction of borate species for $x = 0.50$ and 0.60 are presented in the ESI.†

For the remaining glass compositions, $x = 0.65$–0.80, the molar fraction of $BØO_2^{2-}$ species vanishes and the molar fraction of BO_3^{3-} units can be deduced from the normalized integrated intensity A_2 of the highest-frequency component band with center frequency 1242–1270 cm^{-1} (see Table 2), as follows:

$$X_0 = \frac{A_2}{a_{\text{B−O−}}} = \frac{A_2}{0.785} \tag{17}$$

Then, the molar fraction of borate tetrahedra results from the mass balance equation as $X_4 = 1 - X_0$, where X_4 includes now the new $BØ_2O_2^{3-}$ ortho-borate tetrahedra and the remaining meta-borate $BØ_4^-$ tetrahedra. The results for the short-range borate structure as a function of the bismuth oxide content are presented in Fig. 7.

The IR-derived molar fraction of borate tetrahedra X_4 is compared in Fig. 8a with the reported N_4 values from NMR spectroscopy.[37] It is evident that in the common composition range, between $x = 0.2$ and $x = 0.65$, the IR and NMR data are in good agreement. The experimental X_4 data are also compared in Fig. 8a with the theoretical $N_{4\text{th}}$ value obtained if all oxygen atoms introduced by Bi_2O_3 are forming $BØ_4^-$ units, $N_{4\text{th}} = 3x/(1 - x)$. Clearly, the experimental rate for $BØ_4^-$ formation is considerably lower than $3x/(1 - x)$. For $x = 0.2$ the experimental
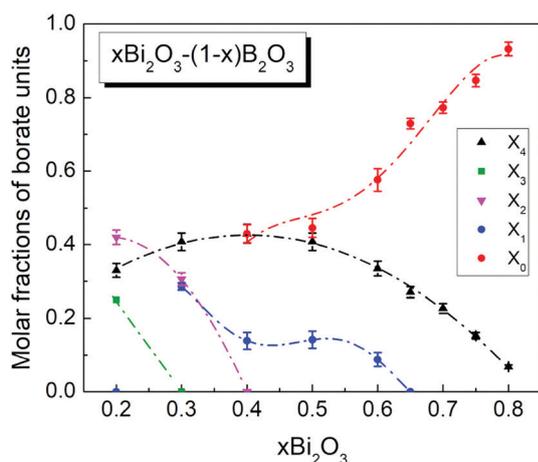

Fig. 8 (a) Comparison of the molar fractions of borate tetrahedral units in glasses $x\text{Bi}_2\text{O}_3$–$(1 - x)\text{B}_2\text{O}_3$ obtained in the present IR study, X_4 (▲), and in the NMR study of ref. 37, N_4 (●). Dashed lines are drawn as guides to the eye. The solid black lines present the theoretical value for the fraction of $BØ_4^-$ units, $N_{4\text{th}}$, formed at rates $3x/(1 - x)$, $1.3x/(1 - x)$ and $x/(1 - x)$. (b) Fractional contributions of the meta-borate tetrahedral units $BØ_4^-$, X_{4m}/X_4, and of the ortho-borate tetrahedral units $BØ_2O_2^{3-}$, X_{4o}/X_4, to the total fraction X_4 of borate tetrahedra in glasses $x\text{Bi}_2\text{O}_3$–$(1 - x)\text{B}_2\text{O}_3$. Solid lines are the fitted exponential curves according to eqn (20).

rate is $1.3x/(1 - x)$, indicating that only 43% of the introduced oxygen forms $BØ_4^-$ units. For $x = 0.3$ the experimental N_4 rate reduces to $x/(1 - x)$, indicating that 33% of the available oxygen forms $BØ_4^-$ units. Therefore, the rest of the added oxygen should participate in other structural arrangements, including the non-bridging oxygen containing $BØ_2O^-$ and $BØO_2^{2-}$ units with molar fractions X_2 and X_1 (Fig. 7).

The last demanding task to fully resolve the short-range borate structure is to separate the contributions of the $BØ_2O_2^{3-}$ and $BØ_4^-$ tetrahedral species to the X_4 values, as resulted from the analysis of the IR spectra. Unfortunately, the characteristic bands of both tetrahedral borate species lie in the 800–1200 cm^{-1} range and overlap strongly; thus, the deconvolution procedure cannot be adopted in this case. Nevertheless, it is possible to evaluate the contributions of the $BØ_2O_2^{3-}$ and $BØ_4^-$ species by observing that at low Bi_2O_3 contents $x = 0.2$ and 0.3 only $BØ_4^-$ species are present and at the highest content, $x = 0.80$, $BØ_2O_2^{3-}$ units prevail as shown in Fig. 3 and 4 and discussed in Section 3.1. Based on the results of Table 2 and the calculated X_4 values, the normalized absorption coefficients a_{4m} and a_{4o} for meta-borate $BØ_4^-$ and ortho-borate $BØ_2O_2^{3-}$ species can be evaluated: $a_{4m} = 0.865 \text{ cm}^{-2}$ and $a_{4o} = 2.440 \text{ cm}^{-2}$. Then, if we denote by X_{4m} and X_{4o} the contributions to the molar fraction X_4 of the meta- and ortho-borate tetrahedra, the following equations result:

$$X_{4m} + X_{4o} = X_4 \quad a_{4m}X_{4m} + a_{4o}X_{4o} = A_{4t} \tag{18}$$

Fig. 7 Molar fractions of the short-range order borate units in glasses $x\text{Bi}_2\text{O}_3$–$(1 - x)\text{B}_2\text{O}_3$ as a function of composition, calculated from data of the deconvoluted absorption coefficient spectra (Fig. 5, 6 and Table 2). Lines are drawn to guide the eye. For details see text.
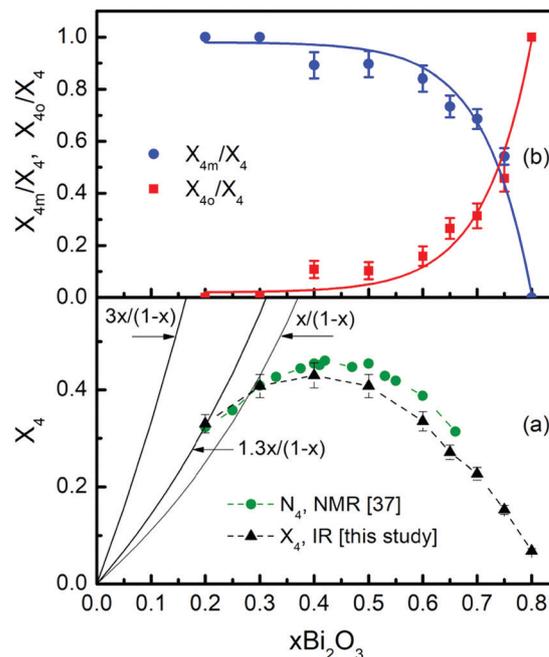
where A_{4t} is the total normalized integrated intensity of the component bands attributed to borate tetrahedral (bands 4–6). Then, solution of eqn (18) gives the molar fractions X_{4m} and X_{4o} as follows:

$$X_{4m} = \frac{a_{4o}X_4 - A_{4t}}{a_{4o} - a_{4m}} = \frac{2.440X_4 - A_{4t}}{1.575}$$

$$X_{4o} = \frac{A_{4t} - a_{4m}X_4}{a_{4o} - a_{4m}} = \frac{A_{4t} - 0.865X_4}{1.575} \quad (19)$$

The fractional contributions of the *meta*-borate, X_{4m}, and the *ortho*-borate, X_{4o}, tetrahedra to the total population of borate tetrahedra X_4 are presented in Fig. 8b. In the same figure are shown also the best fitted curves to the data, according to the exponential formulae:

$$\frac{X_{4m}(x)}{X_4(x)} = A + Be^{Cx}$$

$$\frac{X_{4o}(x)}{X_4(x)} = A' + B'e^{Cx} \quad (20)$$

As shown in Fig. 8b, the relative populations of the $B\varnothing_4^-$ and $B\varnothing_2O_2^{3-}$ species are described well by exponential curves with the constant C in the exponent being $C = 11 \pm 1$, the pre-exponential factors are $B = (-10 \pm 1)10^{-5}$ and $B' = (10 \pm 1)10^{-5}$, and $A = 1$, $A' = 0$.

4.2. Bonding of bismuth in borate glasses

As observed in Fig. 5 and 6, the infrared profiles below 650 cm^{-1} can be described by four component bands. Table 2 shows that the frequencies of these components are in the ranges 162–232 cm^{-1} (band 11), 330–365 cm^{-1} (band 10), 475–510 cm^{-1} (band 9) and 597–615 cm^{-1} (band 8). The latter component (band 8) is related to borate species as it can be assigned to the in-plane bending mode of borate triangular units.[45]

The composition dependence of frequency and relative integrated intensity of bands 9, 10 and 11 are shown in Fig. 9a and b, respectively; relative intensities were obtained by normalizing with the integrated intensity of the entire infrared spectrum. The integrated intensity of band 11 shows an increasing trend up to about $x = 0.60$ and then a tendency for saturation at higher Bi$_2$O$_3$ levels. As noted above, band 11 can be associated to bismuth–oxygen stretching, ν(Bi–O), in ionic sites formed by oxygen atoms provided by the borate network in analogy to previous findings for metal oxide-containing borate glasses.[45,47,48,52,78–81]

Bands 9 and 10 exhibit similar dependences on composition in terms of both frequency and relative intensity. This suggests that these bands can be associated to vibrations of the same bismuthate species, like the BiO$_6$ octahedra discussed in Section 3.2. BiO$_6$ octahedra would have two infrared active T$_{1u}$ modes under O_h point group; the asymmetric stretching (ω_3) and the asymmetric bending (ω_4) modes.[82] Due to structural distortions, the degeneracy of the ω_3 and ω_4 modes will be removed in the glassy state and contribute to broadening of the corresponding bands. Along these lines, we attribute band 9 to
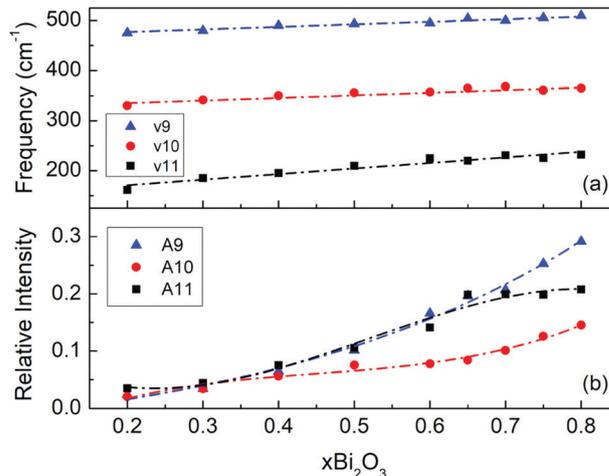

Fig. 9 Composition dependence of frequency (a), and of relative integrated intensity (b) of component bands 9–11 obtained by deconvolution of the infrared spectra of glasses xBi$_2$O$_3$–$(1 - x)$B$_2$O$_3$ (see Fig. 5, 6 and Table 2). Lines are drawn to guide the eye.

the asymmetric stretch (ω_3) and band 10 to the asymmetric bend (ω_4) of distorted BiO$_6$ octahedra in borate glasses. Using frequency data from Table 2 for the ω_4 (ν_{10}) and ω_3 (ν_9) modes of BiO$_6$ octahedra we find an average value of 0.71 for the frequency ratio ω_4/ω_3, in good agreement with the average value $\omega_4/\omega_3 = 0.69$ for octahedral Bi^{3+} complexes.[82]

We note also that the relatively high-frequency value of the ω_3 mode (average 495 cm^{-1}) indicates considerable covalence in the Bi–O bonding. Nevertheless, the corresponding Bi–O bond strength is lower than the average B–O strength as suggested by the large difference in the so-called interaction parameter for the corresponding cation–anion pairs, A_{th}, as determined by Dimitrov and Komatsu;[83] *i.e.* A_{th}(Bi$_2$O$_3$) = 0.008 and A_{th}(B$_2$O$_3$) = 0.244. In addition to this approach, a comparison between the Bi–O and B–O bond strengths can be made by employing experimentally derived values for the weighted average frequency of the ω_3 and ω_4 modes for the BiO$_6$ glass-forming sites, $\nu_{Bi-O(f)} = 451$ cm^{-1}, and the weighted average ν_{B-O} frequency in 4-fold, $\nu_{B-O(4)} = 952$ cm^{-1}, and 3-fold, $\nu_{B-O(3)} = 1292$ cm^{-1}, coordinated boron–oxygen sites. For this, we used frequencies ν_9 and ν_{10} from Table 2 to calculate the weighted average $\nu_{Bi-O(f)}$ value, frequencies ν_4, ν_5 and ν_6 for $\nu_{B-O(4)}$ and frequencies ν_2 and ν_3 for $\nu_{B-O(3)}$.

The harmonic oscillator model for the frequency of vibration of an M–O bond gives $\nu_{M-O} = (1/2\pi c)(k_{M-O}/\mu_{M-O})^{1/2}$ where c is the speed of light and k_{M-O} and μ_{M-O} are the force constant and reduced mass of vibration; this leading to the following expression for M = Bi and M = B:

$$\frac{k_{Bi-O}}{k_{B-O}} = \frac{\mu_{Bi-O}}{\mu_{B-O}} \frac{\nu_{Bi-O}^2}{\nu_{Bi-O}^2} \quad (21)$$

Approximating the reduced mass by $\mu_{M-O} = (m_O m_M)/(m_O + m_M)$ where m is the atomic mass, and considering borate triangular sites with average frequency $\nu_{B-O(3)} = 1292$ cm^{-1}, eqn (21) gives for the glass-forming BiO$_6$ sites $k_{Bi-O(f)} = 0.28k_{B-O(3)}$ using

This journal is © the Owner Societies 2021

Phys. Chem. Chem. Phys., 2021, **23**, 10006–10020 | **10015**

$\nu_{\text{Bi-O}(f)}$ = 451 cm^{-1}. Application of the same equation to ionic bismuth–oxygen sites, which manifest the glass-modifier role of Bi$_2$O$_3$ with an average frequency $\nu_{\text{Bi-O}(m)}$ = 210 cm^{-1}, results in $k_{\text{Bi-O}(m)}$ = 0.06$k_{\text{B-O}(3)}$.

In conclusion, infrared spectroscopy gives values for the average Bi–O bond strength reflecting the dual role of Bi$_2$O$_3$ in borate glasses, *i.e.* as glass-forming and glass-modifying oxide with average Bi–O bond strengths reaching about 28% and 6% of the average B–O bond strength in triangular borate sites.

4.3. Property–structure correlations in bismuth-borate glasses

The strong effect of Bi$_2$O$_3$ on the nature and distribution of structural units constituting the glass, as shown in Fig. 7 and 8, can provide insights into the composition dependence of physical properties. Previous studies focused on the optical basicity and electronic polarizability of bismuth-borate glasses.[28,30] We consider here the glass transition temperature, T_g, a property related to the rigidity of the glass network; the latter reflects the interatomic bonding energy and the atomic packing density of the glass.[84,85]

The composition dependence of T_g is shown in Fig. 10a, based on data reported by Bajaj *et al.*[37] for Bi$_2$O$_3$ contents up to 66 mol% and by George *et al.*[24] for higher Bi$_2$O$_3$ contents (Table 3). Clearly, T_g exhibits a decreasing trend upon increasing Bi$_2$O$_3$ content and the rate of decreasing T_g appears to be composition dependent. In particular, three composition regimes can be distinguished where T_g exhibits approximate linear dependencies on the Bi$_2$O$_3$ content: (I) $0.2 \leq x \leq 0.4$, where T_g decreases at a rather mild rate; (II) $0.4 < x \leq 0.6$, with a fast decrease of T_g; and (III) $0.6 < x \leq 0.83$, where T_g decreases at a reduced rate in comparison to regime II.

The variation of T_g with Bi$_2$O$_3$ content can be viewed in terms of the molar fractions of the short-range units constituting the borate structure (Fig. 7 and 8). The composition range I is characterized by decreasing fractions X_3, X_2 and X_1, while X_4 increases towards its maximum value at $x = 0.4$. The net effect of these structural rearrangements leads apparently to a decreasing connectivity of the borate network as manifested by a slightly decreasing T_g. In region II, the combined effect of decreasing X_4 and the formation of the completely depolymerized *ortho*-borate triangular BO$_3$$^{3-}$ species (X_0) cause a pronounced decrease of T_g. It is of interest to note that in region III the decrease of T_g slows down, despite the continuing decrease of X_4 and the rise of X_0 as observed in Fig. 7. This apparent discrepancy can be resolved by recalling the increasing formation of *ortho*-borate tetrahedral BØ$_2$O$_2$$^{3-}$ species in region III (X_{4o} in Fig. 8). This process restores some of the borate connectivity, because BØ$_2$O$_2$$^{3-}$ provides two bridging boron–oxygen bonds (B–Ø) per boron in comparison to zero B–Ø bonds offered by BO$_3$$^{3-}$ species.

For alkali-borate glasses M$_2$O–2B$_2$O$_3$ (M = Li–Cs), T_g was found to vary proportionally to the average number of bridging B–Ø bonds per boron center, N_b.[86] Using the molar fraction data of this study, N_b can be calculated for bismuth-borate glasses as follows:

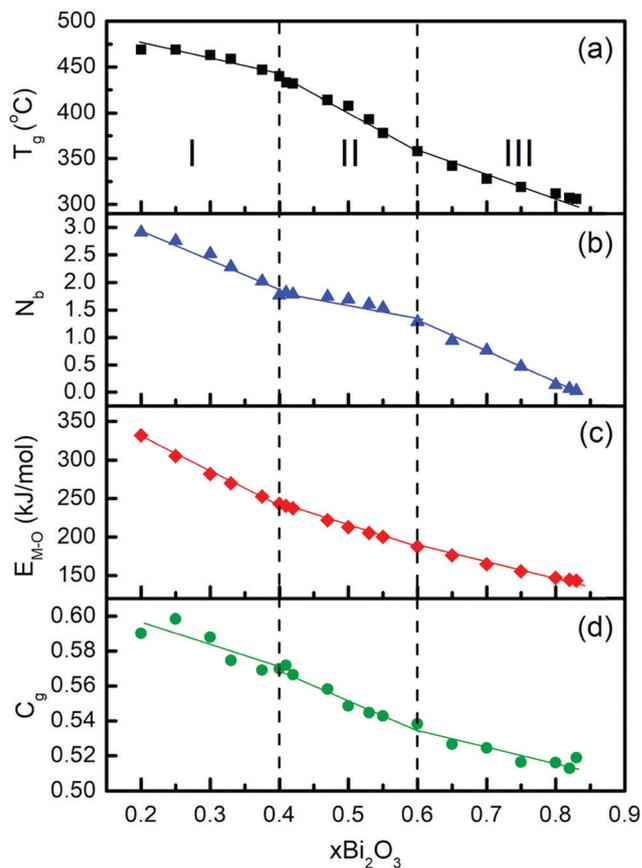$$N_b = 4X_{4m} + 2X_{4o} + 3X_3 + 2X_2 + X_1 \qquad (22)$$

Fig. 10 Composition dependence of properties in glasses xBi$_2$O$_3$–(1 − x)B$_2$O$_3$; (a) glass transition temperature T_g,[24,37] (b) average number of bridging boron–oxygen bonds per boron center N_b, calculated from eqn (22), (c) average single bond strength $E_{\text{M-O}}$, calculated from eqn (24), and (d) atomic packing density, C_g, calculated from eqn (26). Vertical dashed lines mark the Bi$_2$O$_3$ contents x = 0.4 and x = 0.6 which define three regimes (I, II and III) with different rates in the composition dependence of T_g. Straight lines are linear fits to data in the three composition regimes. For details see text.

To calculate N_b for glasses not studied in this work, we used interpolated or extrapolated values for the mole fractions of the borate species involved in eqn (22). The obtained N_b values are plotted in Fig. 10b *versus* Bi$_2$O$_3$ content, and are found to exhibit approximate linear dependencies on composition in the three regimes defined by the T_g response.

As observed in Fig. 10b, the slopes of the N_b variations show differences compared to those of T_g; for example, the decrease of N_b in regime II is not as steep as that of T_g. This indicates that the proportionality constant between T_g and N_b is composition dependent. Also, although N_b plays a crucial role on T_g, there are additional factors which influence T_g as well. They are the strength of the metal cation–oxygen interactions,[87] and the effectiveness in packing of the glass constituents as quantified by the atomic packing density C_g.[84,85]

Previous studies on alkali-borate,[87] alkaline-earth borate,[48] and transition metal-borate[52] glasses, having fixed metal oxide contents, demonstrated linear-dependences of T_g on the strength of the M–O interactions, which express the ability of the M^{n+} cations to cross-link network segments through M–O

10016 | *Phys. Chem. Chem. Phys.*, 2021, **23**, 10006–10020

This journal is © the Owner Societies 2021

Table 3 Selected properties of glasses $x\text{Bi}_2\text{O}_3$–$(1-x)\text{B}_2\text{O}_3$; density d, molar weight M_W, glass transition temperature T_g, average number of bridging boron–oxygen bonds per boron center N_b, average single bond strength $E_{M–O}$, and atomic packing density C_g. Values for N_b, $E_{M–O}$ and C_g were calculated using eqn (22), (24) and (26), respectively

$x\text{Bi}_2\text{O}_3$	d^a (g cm^{-3})	M_W (g mol^{-1})	$T_g{}^a$ (°C)	N_b	$E_{M–O}$ (kJ mol^{-1})	C_g
0.20	4.46	148.89	469	2.91	331.7	0.590
0.25	5.05	168.71	469	2.75	305.4	0.598
0.30	5.47	188.52	463	2.52	282.0	0.588
0.33	5.64	200.41	459	2.28	269.9	0.575
0.375	6.01	218.25	447	2.03	252.7	0.569
0.40	6.25	228.16	440	1.77	243.4	0.570
0.41	6.36	232.12	433	1.82	240.6	0.572
0.42	6.39	236.08	432	1.79	237.3	0.566
0.47	6.74	255.90	414	1.75	221.8	0.558
0.50	6.87	267.79	408	1.70	212.8	0.549
0.53	7.07	279.68	393	1.60	205.2	0.545
0.55	7.21	287.61	378	1.53	200.0	0.543
0.60	7.55	307.42	358	1.28	187.6	0.538
0.65	7.76	327.24	342	0.94	176.3	0.527
0.70	8.10	347.06	328	0.76	164.6	0.524
0.75	8.33	366.88	319	0.47	155.3	0.516
0.80	8.67	386.69	312	0.14	146.9	0.516
0.82	8.75	394.62	307	0.06	144.4	0.513
0.83	8.92	398.58	306	0.03	143.1	0.519

^{a} Density and glass transition temperature data are from Bajaj et al.[37] for Bi_2O_3 contents up to 66 mol% and from George et al.[24] for higher Bi_2O_3 contents.

bonding. Instead of looking separately at the effects of metal cation–oxygen (*i.e.*, Bi–O) and B–O bonding on T_g, we propose to evaluate their combined effect on the interatomic bonding energy of the glass determining the rigidity of the glass network, in terms of the average single bond energy $E_{M–O}$ calculated as follows:

$$E_{M–O} = \frac{x}{3(1+x)}\left[6\left(1-f_{Bi–O(f)}\right)E_{Bi–O(m)} + 6f_{Bi–O(f)}E_{Bi–O(f)}\right]$$
$$+ \frac{(1-x)}{3(1+x)}\left[4X_4 E_{B–O(4)} + 3(1-X_4)E_{B–O(3)}\right] \tag{23}$$

The above equation takes into consideration the coordination numbers of bismuth and boron. For boron, information for 4-fold (X_4) and 3-fold ($1-X_4$) coordination is taken from the present IR results. Bismuth is assumed to have six-fold coordination in both glass-modifying and glass-forming sites,[25] with the fraction of Bi in the latter sites being obtained from the corresponding far-IR relative intensity: $f_{Bi–O(f)} = (A_9 + A_{10})/(A_9 + A_{10} + A_{11})$. The terms $E_{Bi–O(m)}$, $E_{Bi–O(f)}$, $E_{B–O(4)}$, and $E_{B–O(3)}$ denote the average bond energies in the corresponding Bi–O and B–O sites. Considering that $k_{Bi–O(m)} = 0.06k_{B–O(3)}$ and $k_{Bi–O(f)} = 0.28k_{B–O(3)}$, and the relation $k_{B–O(4)} = 0.54k_{B–O(3)}$ between three- and four-fold borate sites, eqn (23) can be simplified to read:

$$E_{M–O} = \frac{x}{3(1+x)}\left[0.36 + 1.32f_{Bi–O(f)}\right]E_{B–O(3)}$$
$$+ \frac{(1-x)}{3(1+x)}\left[3 - 0.84X_4\right]E_{B–O(3)} \tag{24}$$

For the average single B–O bond energy in three-fold borate sites we use $E_{B–O(3)} = 498$ kJ mol^{-1} [28] and apply eqn (24) to

calculate the average single bond energy, $E_{M–O}$, in glasses $x\text{Bi}_2\text{O}_3$–$(1-x)\text{B}_2\text{O}_3$. The results are given in Table 3 and plotted in Fig. 10c as a function of composition. It is found that consideration of both borate and bismuthate constituents leads to a rather smooth decrease in the average single bond energy with Bi_2O_3 content. Nevertheless, progressive changes in the slop of $E_{M–O}$ *versus* Bi_2O_3 content can still be seen in the three composition regimes. In any case, the variation of $E_{M–O}$ with composition is in line with the general trends of both T_g and N_b.

Finally, we evaluate the composition dependence of the atomic packing density C_g in bismuth-borate glasses. C_g is defined as the ratio between the theoretical volume occupied by the constituent ions and the real volume of glass. For multicomponent glasses C_g is given by the general equation:

$$C_g = d\frac{\frac{4}{3}\pi N_A \sum f_i\left(ar_A{}^3 + br_B{}^3\right)}{\sum f_i M_i} \tag{25}$$

where d is the glass density, N_A is the Avogadro number, and f_i is the molar fraction of the ith glass component having chemical formula A_aB_b, molar mass M_i, and ionic radii r_A and r_B for atoms A and B, respectively.[85] For glasses $x\text{Bi}_2\text{O}_3$–$(1-x)\text{B}_2\text{O}_3$, eqn (25) reduces to the form:

$$C_g = d\frac{\frac{4}{3}\pi N_A\left(2xr_{Bi}{}^3 + 2(1-x)r_B{}^3 + 3r_O{}^3\right)}{M_W} \tag{26}$$

Values of density (d) and molar weight (M_W) are given in Table 3, noting that the ratio d/M_W in eqn (26) is the inverse of the glass molar volume, $1/V_m$. For radii we use effective ionic radii of Shannon,[88] taking the values $r_O = 1.35$ Å for oxygen and $r_{Bi} = 1.03$ Å for bismuth, the latter corresponding to Bi in six-fold coordination. For the ionic radius of boron we take into consideration the change in coordination number with composition (x) and write $r_B = X_4 r_{B(4)} + (1 - X_4)r_{B(3)}$,[89] where the boron ionic radii for 4- and 3-fold coordination are $r_{B(4)} = 0.11$ Å and $r_{B(3)} = 0.01$ Å;[88] recognizing though that boron has a very small effect on C_g in comparison to oxygen and bismuth.

The calculated C_g values are given in Table 3, while the evolution of the atomic packing density with composition is demonstrated in Fig. 10d. Despite the fact that the C_g values seem to have relatively larger scattering than those for N_b and $E_{M–O}$, all three properties are found to exhibit a general decreasing trend with Bi_2O_3 content. It is noted though that C_g shows a maximum at $x = 0.25$, which should reflect the minimum in V_m at the same composition as reported by George *et al.*[24] In any case, it is found that N_b, $E_{M–O}$ and C_g all contribute to shaping the overall composition dependence of T_g (Fig. 10a). Considering that the glass structure affects directly N_b, $E_{M–O}$ and C_g as expressed by eqn (22), (24) and (26), the present results demonstrate the close correlation between T_g and glass structure in the broad glass-forming region of the bismuth-borate system.

5. Conclusions

Glasses in the system $x\text{Bi}_2\text{O}_3$–$(1 - x)\text{B}_2\text{O}_3$ were synthesized by melting in Pt crucibles and subsequent splat-quenching between two stainless-steel blocks; this technique was found to give homogeneous glasses in the continuous range $0.2 \leq x \leq 0.8$. The evolution of glass structure with composition (x) was studied by infrared (IR) reflectance spectroscopy in a broad and continuous spectral range, comprising well-separated far- (30–650 cm^{-1}) and mid-IR (650–5000 cm^{-1}) responses for bismuth-borate glasses. Absorption coefficient spectra were calculated from the measured reflectance spectra, and were deconvoluted into component bands attributed to vibration modes of specific bismuthate and borate species.

The Bi–O vibrational activity was probed at low frequencies in the far-IR region. It involves a band at 160–230 cm^{-1} due to Bi–O stretch in ionic sites reflecting the glass-modifying role of Bi$_2$O$_3$, and bands at 330–365 cm^{-1} and 475–510 cm^{-1} assigned to the asymmetric bend and asymmetric stretch in distorted BiO$_6$ sites. The relatively high frequency of the latter bands demonstrates considerable covalence in the Bi–O bonding in BiO$_6$ sites and manifests the parallel glass-forming role of Bi$_2$O$_3$. Ionic Bi–O and relatively covalent BiO$_6$ sites were found to coexist in the composition region $0.20 \leq x \leq 0.80$. The latter sites prevail for Bi$_2$O$_3$ contents above 60 mol%, and account for the extended glass-forming range of the bismuth-borate system. Consideration of the corresponding IR frequencies allowed estimating the average Bi–O bond strengths in glass-modifying and glass-forming bismuthate sites; they reach *ca.* 6% and 28% of the average B–O bond strength in triangular borate sites.

Bands arising from B–O stretching modes were found in the 810–1090 cm^{-1} and 1155–1490 cm^{-1} range for borate units having tetrahedral and triangular B–O coordination, while their bending modes are active in the 595–710 cm^{-1} range. Comparison with previous IR studies on modified borate glasses and bismuth-borate crystalline compounds allowed the borate speciation as a function of composition. Thus, two kinds of borate tetrahedral species were identified having the *meta*-borate, BØ$_4^-$, and *ortho*-borate, BØ$_2$O$_2^{3-}$, stoichiometry where the oxygen atoms are all bridging (Ø) or two are bridging and two non-bridging (O$^-$), respectively. In addition, all possible types of triangular borate units were identified in bismuth-borate glasses for the first time, *i.e.* units BØ$_3$, BØ$_2$O$^-$, BØO$_2^{2-}$ and BO$_3^{3-}$ with increasing number of non-bridging oxygen atoms per boron. The IR results on the relative integrated intensity of bands characterizing the different borate species were combined with mass and charge balance equations to quantify for the first time all six type of borate species present in the bismuth-borate glass system. The complete mapping of the short-range borate structure as a function of composition was achieved in terms of the molar fractions X_{4m}, X_{4o}, X_3, X_2, X_1 and X_0 of units BØ$_4^-$, BØ$_2$O$_2^{3-}$, BØ$_3$, BØ$_2$O$^-$, BØO$_2^{2-}$ and BO$_3^{3-}$, respectively. The present IR results for the total molar fraction X_4 of the borate tetrahedral species, $X_4 = X_{4m} + X_{4o}$, were found in excellent agreement with reported N_4 data from NMR

spectroscopy.[37] In addition to X_4 or N_4, the present work gives the X_{4m} and X_{4o} fractions as well as the fractions of all types of triangular borate species X_{3-n} where n = 0, 1, 2 and 3.

The composition dependence of the glass transition temperature, T_g, of bismuth-borate glasses[24,37] was discussed in terms of three glass properties calculated using the structural results of this work: the average number of bridging boron–oxygen bonds (B–Ø) per boron center, N_b, the average Bi–O and B–O single bond energy, E_{M-O}, and the atomic packing density, C_g. It was found that N_b, E_{M-O} and C_g all exhibit approximate linear dependencies on the Bi$_2$O$_3$ content in the three composition regimes $0.2 \leq x \leq 0.4$, $0.4 < x \leq 0.6$ and $0.6 < x \leq 0.83$, and contribute to the overall composition dependence of T_g. In conclusion, T_g-structure correlations are determined by the combined effect of the borate cross-linking ability, the strength of the interatomic bonding energy and the effectiveness of atomic packing in the studied bismuth-borate glasses.

Author contributions

C. P. E. Varsamis: conceptualization, software, formal analysis, writing – original draft. N. Makris: investigation, formal analysis. C. Valvi: investigation, formal analysis. E. I. Kamitsos: conceptualization, supervision, funding acquisition, writing – review & editing, project administration.

Conflicts of interest

There are no conflicts of interest to declare.

Acknowledgements

References

1 M. B. Saisudha, K. S. R. K. Rao, H. L. Bhat and J. Ramakrishna, *J. Appl. Phys.*, 1996, **80**, 4845–4853.

2 G. S. Murugan and K. B. R. Varma, *J. Non-Cryst. Solids*, 2001, **279**, 1–13.

3 P. Becker, *Cryst. Res. Technol.*, 2003, **38**, 74–82.

4 Y. Chen, Y. Huang, M. Huang, R. Chen and Z. Luo, *Opt. Mater.*, 2004, **25**, 271–278.

5 I. I. Oprea, H. Hesse and K. Betzler, *Opt. Mater.*, 2004, **26**, 235–237.

6 R. Ihara, T. Honma, Y. Benino, T. Fujiwara and T. Komatsu, *Opt. Mater.*, 2004, **27**, 403–408.

10018 | *Phys. Chem. Chem. Phys.*, 2021, **23**, 10006–10020

This journal is © the Owner Societies 2021

7 R. Ihara, Y. Benino, T. Fujiwara and T. Komatsu, *Sci. Technol. Adv. Mater.*, 2005, **6**, 138–142.

8 O. Deparis, F. P. Mezzapesa, C. Corbari, P. G. Kazansky and K. Sakaguchim, *J. Non-Cryst. Solids*, 2005, **351**, 2166–2177.

9 A. S. L. Gomez, E. L. Falcão Filho, C. B. de Araújo, D. Rativa, R. E. de Araujo, K. Sakaguchi, F. P. Mezzapesa, I. C. S. Carvalho and P. G. Kazansky, *J. Appl. Phys.*, 2007, **101**, 033115.

10 S. Insitipong, J. Kaewkhao, T. Ratana and P. Limsuwan, *Procedia Eng.*, 2011, **8**, 195–199.

11 K. Swapna, Sk Mahamuda, A. Srinivasa Rao, M. Jayasimhadri, T. Sasikala and L. Rama Moorthy, *Ceram. Interfaces*, 2013, **39**, 8459–8465.

12 K. Swapna, S. Mahamuda, A. Srinivasa Rao, T. Sasikala, P. Packiyaraj, L. Rama Moorthy and G. V. Prakash, *J. Luminescence*, 2014, **156**, 80–86.

13 K. Swapna, S. Mahamuda, A. Srinivasa Rao, M. Jayasimhadri, S. Shakya and G. Vijaya Prakash, *J. Luminescence*, 2014, **156**, 180–187.

14 S. Singla, V. G. Achanta, N. Mahendru, S. S. Prabhu, M. Falconieri and G. Sharma, *Opt. Mater.*, 2017, **72**, 91–97.

15 B. Munisudhakar, C. Nageswara Raju, M. Reddi Babu, N. Manohar Reddy and L. Rama Moorthy, *Mater. Today: Proc.*, 2020, **26**, 5–10.

16 M. G. Dong, M. I. Sayyed, G. Lakshminarayana, M. Çelikbilek Ersundu, A. E. Ersundu, P. Nayar and M. A. Mahdi, *J. Non-Cryst. Solids*, 2017, **468**, 12–16.

17 M. I. Sayyed, G. Lakshminarayana, M. G. Dong, M. Çelikbilek Ersundu, A. E. Ersundu and I. V. Kityk, *Radiat. Phys. Chem.*, 2018, **145**, 26–33.

18 P. Kaur, K. J. Singh, S. Thakur, P. Singh and B. S. Bajwa, *Spectrochim. Acta, Part A*, 2019, **206**, 367–377.

19 D. W. Hall, M. A. Newhouse, N. F. Borrelli, W. H. Dumbaugh and D. L. Weidman, *Appl. Phys. Lett.*, 1989, **54**, 1293–1295.

20 E. M. Levin and C. L. McDaniel, *J. Am. Ceram. Soc.*, 1962, **45**, 355–360.

21 H. Hellwig, J. Liebertz and L. Bohaty, *Solid State Commun.*, 1999, **109**, 249–251.

22 H. Hellwig, J. Liebertz and L. Bohaty, *J. Appl. Phys.*, 2000, **88**, 240–244.

23 C. Stehle, C. Vira, D. Hogan, S. Feller and M. Affatigato, *Phys. Chem. Glasses*, 1998, **39**, 83–86.

24 H. B. George, C. Vira, C. Stahle, J. Meyer, S. Evers, D. Hogan, S. Feller and M. Affatigato, *Phys. Chem. Glasses*, 1999, **40**, 326–332.

25 K. Terashima, T. H. Shimoto and T. Yoko, *Phys. Chem. Glasses*, 1997, **38**, 211–217.

26 P. Becker, *Adv. Mater.*, 1998, **10**, 979–992.

27 Y. Watanabe, S. Sakata, T. Watanabe and T. Tsuchiya, *J. Non-Cryst. Solids*, 1998, **240**, 212–220.

28 T. Komatsu, N. Ito, T. Honma and V. Dimitrov, *J. Non-Cryst. Solids*, 2010, **356**, 2310–2314.

29 B. V. R. Chowdari and Z. Rong, *Solid State Ionics*, 1996, **90**, 151–160.

30 T. Honma, Y. Benino, T. Komatsu, R. Sato and V. Dimitrov, *Phys. Chem. Glasses*, 2002, **43**, 32–40.

31 C. E. Stone, A. C. Wright, R. N. Sinclair, S. A. Feller, M. Affatigato, D. L. Hogan, N. D. Nelson, C. Vira, Y. B. Dimitriev, E. M. Gattef and D. Ehrt, *Phys. Chem. Glasses*, 2000, **41**, 409–412.

32 L. Baia, R. Stefan, W. Kiefer, J. Popp and S. Simon, *J. Non-Cryst. Solids*, 2002, **303**, 379–386.

33 L. Baia, R. Stefan, J. Popp, S. Simon and W. Kiefer, *J. Non-Cryst. Solids*, 2003, **324**, 109–117.

34 B. Karthikeyan and S. Mohan, *Phys. B*, 2003, **334**, 298–302.

35 A. V. Egorysheva, V. I. Burkov, Yu. F. Kargin, V. G. Plotnichenko and V. V. Koltashev, *Crystallogr. Rep.*, 2005, **50**, 127–136.

36 L. Baia, R. Stefan, W. Kiefer and S. Simon, *J. Raman Spectrosc.*, 2005, **36**, 262–266.

37 A. Bajaj, A. Khanna, B. Chen, J. G. Longstaffe, U. W. Zwanziger, J. W. Zwanziger, Y. Gomez and F. Gonzalez, *J. Non-Cryst. Solids*, 2009, **355**, 45–53.

38 N. M. Bobkova, *Glass Ceram.*, 2015, **72**, 360–365.

39 G. E. Jellison, S. A. Feller and P. J. Bray, *Phys. Chem. Glasses*, 1978, **19**, 52.

40 S. A. Feller, W. J. Dell and P. J. Bray, *J. Non-Cryst. Solids*, 1982, **51**, 21–30.

41 R. E. Youngman and J. W. Zwanziger, *J. Non-Cryst. Solids*, 1994, **168**, 293–297.

42 R. E. Youngman and J. W. Zwanziger, *J. Phys. Chem.*, 1996, **100**, 16720–16728.

43 S. A. Feller, *Phys. Chem. Glasses: Eur. J. Glass Sci. Technol., Part B*, 2018, **59**, 153–167.

44 E. I. Kamitsos, M. A. Karakassides and G. D. Chryssikos, *Phys. Chem. Glasses*, 1989, **30**, 229–234.

45 E. I. Kamitsos, A. P. Patsis, M. A. Karakassides and G. D. Chryssikos, *J. Non-Cryst. Solids*, 1990, **126**, 52–67.

46 E. I. Kamitsos and G. D. Chryssikos, *J. Mol. Struct.*, 1991, **247**, 1–16.

47 C. P. Varsamis, E. I. Kamitsos and G. D. Chryssikos, *Phys. Rev. B: Condens. Matter Mater. Phys.*, 1999, **60**, 3885–3898.

48 Y. D. Yiannopoulos, G. D. Chryssikos and E. I. Kamitsos, *Phys. Chem. Glasses*, 2001, **42**, 164–172.

49 C. P. E. Varsamis, A. Vegiri and E. I. Kamitsos, *Phys. Rev. B: Condens. Matter Mater. Phys.*, 2002, **65**, 104203.

50 E. I. Kamitsos, *Phys. Chem. Glasses*, 2003, **44**, 79–87.

51 A. Winterstein-Beckmann, D. Möncke, D. Palles, E. I. Kamitsos and L. Wondraczek, *J. Phys. Chem. B*, 2015, **119**, 3259–3272.

52 D. Möncke, E. I. Kamitsos, D. Palles, R. Limbach, A. Winterstein-Beckmann, T. Honma, Z. Yao, T. Rouxel and L. Wondraczek, *J. Chem. Phys.*, 2016, **145**, 124501.

53 A. C. Wright, *Phys. Chem. Glasses: Eur. J. Glass Sci. Technol., Part B*, 2010, **51**, 1–39.

54 G. Lelong, L. Cormier, L. Hennet, F. Michel, J.-P. Rueff, J. M. Ablett and G. Monaco, *J. Non-Cryst. Solids*, 2017, **472**, 1–8.

55 M. S. Bødker, J. C. Mauro, R. E. Youngman and M. M. Smedskjaer, *J. Phys. Chem. B*, 2019, **123**, 1206–1213.

56 G. Ferlat, T. Charpentier, A. P. Seitsonen, A. Takada, M. Lazzeri, L. Cormier, G. Calas and F. Mauri, *Phys. Rev. Lett.*, 2008, **101**, 065504.

This journal is © the Owner Societies 2021

Phys. Chem. Chem. Phys., 2021, **23**, 10006–10020 | **10019**

57 E. I. Kamitsos, Y. D. Yiannopoulos, C. P. Varsamis and H. Jain, *J. Non-Cryst. Solids*, 1997, **222**, 59–68.

58 O. Sanz, E. Haro-Poniatowski, J. Gonzalo and J. M. Fernandez Navarro, *J. Non-Cryst. Solids*, 2006, **352**, 761–768.

59 C. P. Varsamis, E. I. Kamitsos, N. Machida and T. Minami, *J. Phys. Chem. B*, 1997, **101**, 3734–3741.

60 J. J. More, *Lect. Notes Math.*, 1978, **630**, 105–116.

61 A. Winterstein-Beckmann, D. Möncke, D. Palles, E. I. Kamitsos and L. Wondraczek, *J. Non-Cryst. Solids*, 2013, **376**, 165–174.

62 G. Chadeyron, M. El-Ghozzi, R. Mahiou, A. Arbus and J. C. Cousseins, *J. Solid State Chem.*, 1997, **128**, 261–266.

63 M. Ren, J. H. Lin, Y. Dong, L. Q. Yang and M. Z. Su, *Chem. Mater.*, 1999, **11**, 1576–1580.

64 R. Velchuri, B. V. Kumar, V. R. Devi, G. Prasad, D. J. Prakash and M. Vithal, *Mater. Res. Bull.*, 2011, **46**, 1219–1226.

65 C. P. E. Varsamis, E. I. Kamitsos, M. Tatsumisago and T. Minami, *J. Non-Cryst. Solids*, 2004, **345&346**, 93–98.

66 A. V. Egorysheva, A. S. Kanishcheva, Yu. F. Kargin, Yu. E. Gorbunova and Yu. N. Mikhailov, *Z. Neorg. Chim.*, 2002, **47**, 1961–1965.

67 G. M. Kuzmicheva and T. I. Mel'nikova, *Z. Neorg. Chim.*, 2009, **54**, 74–81.

68 S. Filatov, Y. Shepelev, R. Bubnova, N. Sennova, A. V. Egorysheva and Y. F. Kargin, *J. Solid State Chem.*, 2004, **177**, 515–522.

69 P. Becker and R. Frohlich, *Z. Naturforsch.*, 2004, **59b**, 256–258.

70 A. Hyman and A. Perloff, *Acta Crystallogr., Sect. B: Struct. Crystallogr. Cryst. Chem.*, 1972, **28**, 2007–2011.

71 R. J. Betsch and W. B. White, *Spectrochim. Acta, Part A*, 1978, **34**, 505–514.

72 R. Iordanova, V. Dimitrov, Y. Dimitriev and D. Klissurski, *J. Non-Cryst. Solids*, 1994, **180**, 58–65.

73 R. Iordanova, Y. Dimitriev, V. Dimitrov, S. Kassabov and D. Klissurski, *J. Non-Cryst. Solids*, 1996, **204**, 141–150.

74 S. Hazra, S. Mandal and A. Ghosh, *Phys. Rev. B: Condens. Matter Mater. Phys.*, 1997, **56**, 8021–8025.

75 N. Kitamura and K. Fukumi, *J. Ceram. Soc. Jpn.*, 2013, **121**, 355–360.

76 F. Miyaji, T. Yoko, J. Jin, S. Sakka, T. Fukunaga and M. Misawa, *J. Non-Cryst. Solids*, 1994, **175**, 211–223.

77 Y. Dimitriev, Ch Petkov, E. Gattev, T. Stoilova and G. Gochev, *J. Non-Cryst. Solids*, 1989, **112**, 120–125.

78 J. A. Duffy, E. I. Kamitsos, G. D. Chryssikos and A. P. Patsis, *Phys. Chem. Glasses*, 1993, **34**, 153–157.

79 E. I. Kamitsos, G. D. Chryssikos, A. P. Patsis and J. A. Duffy, *J. Non-Cryst. Solids*, 1996, **196**, 249–254.

80 Z. Y. Yao, D. Möncke, E. I. Kamitsos, P. Houizot, F. Célarié, T. Rouxel and L. Wondraczek, *J. Non-Cryst. Solids*, 2016, **435**, 55–68.

81 E. I. Kamitsos, C. P. E. Varsamis and A. Vegiri, *Phys. Chem. Glasses: Eur. J. Glass Sci. Technol., Part B*, 2020, **61**, 107–120.

82 K. Nakamoto, *Infrared and Raman Spectra of Inorganic and Coordination Compounds, Part A, Theory and Applications in Inorganic Chemistry*, Wiley, New York, 6th edn, 2009.

83 V. Dimitrov and T. Komatsu, *J. Ceram. Soc. Jpn.*, 1999, **107**, 1012–1018.

84 T. Rouxel, *J. Am. Ceram. Soc.*, 2007, **90**, 3019–3039.

85 A. Makishima and J. D. Mackenzie, *J. Non-Cryst. Solids*, 1973, **12**, 35–45.

86 E. I. Kamitsos, A. P. Patsis and G. D. Chryssikos, *J. Non-Cryst. Solids*, 1993, **152**, 246–257.

87 E. I. Kamitsos, G. D. Chryssikos and M. A. Karakassides, *Phys. Chem. Glasses*, 1988, **29**, 121–126.

88 R. D. Shannon, *Acta Crystallogr., Sect. A: Found. Crystallogr.*, 1976, **32**, 751–767.

89 N. S. Tagiara, E. Moayedi, A. Kyritsis, L. Wondraczek and E. I. Kamitsos, *J. Phys. Chem. B*, 2019, **123**, 7905–7918.

10020 | *Phys. Chem. Chem. Phys.*, 2021, **23**, 10006–10020

This journal is © the Owner Societies 2021